

# Generative Adversarial Network to Learn Valid Distributions of Robot Configurations for Inverse Kinematics and Constrained Motion Planning

Teguh Santoso Lembono<sup>1,2</sup>, Emmanuel Pignat<sup>1,2</sup>, Julius Jankowski<sup>1,2</sup>, and Sylvain Calinon<sup>1,2</sup>

**Abstract—** In high dimensional robotic system, the manifold of the valid configuration space often has complex shape, especially under constraints such as end-effector orientation, static stability, and obstacles. We propose a generative adversarial network approach to learn the distribution of valid robot configurations. It can generate configurations that are close to the constraint manifold. We present two applications of this method. First, by learning the conditional distribution with respect to the desired end-effector position, we can do fast inverse kinematics even for very high degrees-of-freedom (DoF) systems. Then, it can be used to generate samples in sampling based constrained motion planning algorithms to reduce the necessary projection steps, speeding up computation. We validate the approach in simulation using the 7-DoF Panda manipulator and the 28-DoF humanoid robot Talos.

## I. INTRODUCTION

Generative Adversarial Network (GAN) [1] is a powerful method to learn complex distributions. It is particularly popular in computer vision, where it is used to learn the distribution of images in the dataset. Some of the applications include generating high resolution images [2], text-to-image synthesis [3], and interactive art [4]. We propose to adapt GAN to the context of robotics, by learning the distribution of valid robot configurations in constraint manifolds.

In robotics, the configuration space refers to the space of possible robot configurations that may include joint angles for revolute joints, joint translations for prismatic joints, and the base pose for floating-based robots. This concept is very important in motion planning, because planning a robot path often needs to be done in the configuration space. Due to the presence of constraints, the valid configurations lie in some manifold of the configuration space, the shape of which can be complicated and often cannot be parameterized explicitly. Inequality constraints, such as obstacle avoidance, result in a manifold with non-zero volume, and the standard approach to sample from this manifold is to do rejection sampling. For equality constraints (such as fixed feet locations, or end-effector orientation), however, the manifold volume is reduced to zero, as the manifold has lower dimension than the original space. In this case, rejection sampling does not work because there is zero probability that the random sample will be on the manifold. A common approach is to project the random samples to the manifold, and this projection

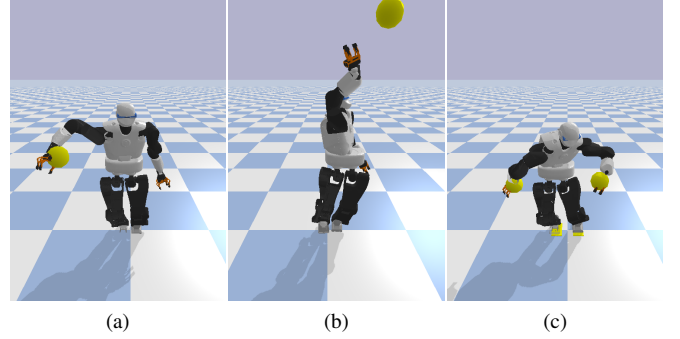


Fig. 1. Using GAN for obtaining approximate IK solutions. The targets are depicted in yellow. In (a), the target is reachable. When the target is out of reach (b), GAN still outputs a configuration close to the constraint manifold. We can also give the four limbs position as the IK targets (c).

step takes a significant portion of the planning computation time. By using GAN to learn the distribution of valid robot configurations in the manifold, we show that we can sample from this manifold effectively. The generated samples will be quite close to the manifold, and the subsequent projection steps are much faster than random sampling.

Having learned the valid distributions, we show that it can be used in two applications: inverse kinematics (IK) and sampling-based constrained motion planning. Analytical IK is typically only available for robots with 6-DoF or lower. For higher DoF robots, the most common method is to use numerical IK, where we start with an initial robot configuration (often selected randomly), and rely on optimization to find the configuration that reach the desired end-effector pose while satisfying the constraints. In our proposed framework, by including the end-effector target position as additional input to the generator, we can obtain configurations that are close to achieving the target. We compare this against doing IK based on random samples, and show that our approach is faster and has higher success rate. Furthermore, sampling-based constrained motion planning also involves high numbers of projections of random samples to the constraint manifold. We show that by replacing the random sampling with the GAN framework, the planning time can be reduced significantly.

One particular difficulty of learning a distribution is when the target distribution is multimodal, as it is the case in many robotic systems. For example, the conditional distribution of a 6-DoF manipulator given a desired end-effector pose is

<sup>1</sup> Idiap Research Institute, Martigny, Switzerland <sup>2</sup> EPFL, Lausanne, Switzerland {name.surname}@idiap.ch

This work was supported by the European Commission's Horizon 2020 Programme (MEMMO project, <http://www.memmo-project.eu/>, grant 780684).

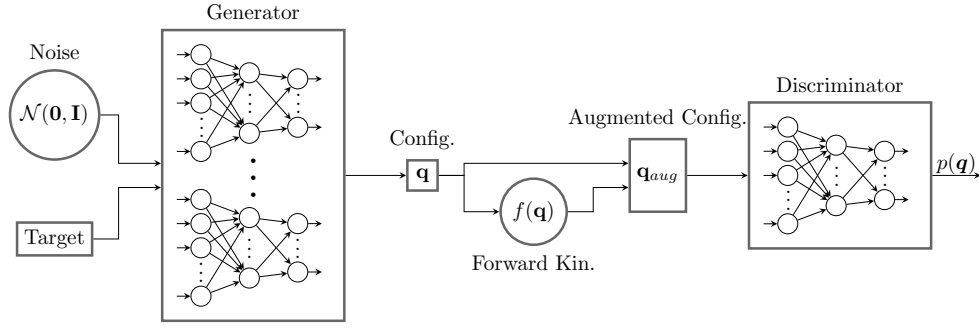


Fig. 2. The proposed GAN framework for learning the distribution of valid robot configurations. The generator consists of an ensemble of  $N_{net}$  neural networks, while the discriminator consists of a single neural network. Besides a Gaussian noise as in standard GAN, we also add the end-effector target(s) as additional input to the generator. The output of the generator is then augmented by additional features, i.e. the corresponding end-effector poses, before being given to the discriminator.

multimodal, because there are many qualitatively different configurations that are associated with the pose. To overcome this, we propose to use an ensemble of neural networks as the generator in GAN. Each neural network can converge to a different mode, and we get better coverage of the distribution as compared to using a single network.

The remainder of the paper is as follows. In Section II, we review existing work on learning sampling distributions and constrained-based motion planning. Section III describes the GAN framework, and how we use it for inverse kinematics and constrained motion planning. The experiments with 7-DoF Panda and 28-DoF Talos are presented in Section IV. Finally, we conclude with a few remarks in Section V.

## II. RELATED WORK

### A. Learning sampling distribution

In [5], [6], Gaussian Mixture Model (GMM) is used to learn the sampling distributions based on previously planned paths. The distribution is used to either generate biased samples for the sampling algorithm, or to construct a repetition roadmap that guides towards finding the solution. It speeds up the computation as compared to uniform sampling, but it is difficult to generalize it to different situations (e.g. different obstacles). Also, GMM does not scale well to higher dimensional systems. Conditional Variational Autoencoder (CVAE) is used in [7], also trained based on data from demonstrations or planned paths, but it is not implemented on constrained system. Convolutional Autoencoder is used in [8] to learn the motion manifold of human motion, but not in the context of motion planning. In contrast, we propose to use Generative Adversarial Network (GAN) to learn the sampling distribution of constrained robotic systems. GAN scales better with higher dimension as compared to GMM, and it is easy to have conditional distribution with respect to some task (such as end-effector pose) by including the task as additional input to the generator in GAN.

### B. Constrained motion planning

A review of various approaches in sampling-based motion planning for constrained systems can be found in [9]. Among the others, projecting the samples to the constraint manifold

is a simple but very generalizable way of extending the standard Rapidly-exploring Random Tree (RRT) to constrained problems. Instead of doing rejection sampling, the samples are projected to the constraints manifold [10], [11]. While it works well, the projection steps take most of the planning time. In [12], Yang *et al.* compare various algorithms for motion planning of humanoid robot. They report that the projection step takes more than 95% of the planning time. Several research lines attempt to reduce this time computation. For example, in [13], Stilman *et al.* use the tangential direction of the constraint manifold to always move while staying close to the manifold. In [14], Kanehiro *et al.* simplify the humanoid structure by splitting it into multiple 6-DoF structures, and then perform analytical IK.

In our proposed method, we are able to generate samples that are already close to the constraints manifold, and the approach is generalizable to most robotic systems. This will reduce the necessary projection step significantly, hence lowering computation time. Additionally, optimization-based approaches such as TrajOpt [15] can solve constrained planning quickly by including the constraints in the optimization problem. However, since the problem is highly nonlinear, these methods often require good initial guesses, otherwise they may have lower success rate even for simple problems [16]. In contrast, sampling-based motion planning can find a global solution with probabilistic completeness guarantee [11].

## III. METHOD

In this section, we present the proposed GAN framework for learning the robot distribution, including some changes as compared to a standard GAN. We then propose two applications: inverse kinematics and constrained motion planning.

### A. Generative Adversarial Framework

In the generative adversarial framework [1], a generator  $G(\mathbf{z}; \theta_G)$  is trained to transform the input noise  $\{\mathbf{z}\}$  drawn from  $p_z(\mathbf{z})$  into samples  $\{\mathbf{q}\}$  that look similar to the data distribution. To do this, a discriminator  $D(\mathbf{q}; \theta_D)$  is trained in parallel to output the probability  $p(\mathbf{q})$  that tells whether  $\mathbf{q}$  comes from the dataset or the generator. The training of

GAN is therefore like a game between the generator and the discriminator, where one tries to beat the other. The generator and discriminator are typically neural networks (with parameters  $\theta_G$  and  $\theta_D$ , respectively) trained with Stochastic Gradient Descent (SGD). In our approach, GAN is trained to generate robot configurations  $\{q\}$  that lie in the desired constraints manifold. The following sections explain some changes to standard GAN that we propose to better suit robotic applications. Unlike in images, we can incorporate several forms of prior knowledge of what constitutes good configurations, in the form of additional cost functions and transformations. To better handle multimodal distributions, we use an ensemble of neural networks as the generator. The framework is depicted in Fig. I.

1) *Additional inputs*: In standard GAN, the input to the generator is a noise sampled from a Gaussian distribution. To obtain conditional distribution, we include the task parameters as additional inputs to the generator. The task parameters in this case correspond to the desired end-effector pose, but other additional tasks are also possible.

2) *Additional costs*: The training cost for the generator normally consists of the cost of tricking the discriminator to classify its samples as dataset samples. In robotics, however, we can add other costs that can be used to evaluate the quality of the samples, based on the knowledge of the robotic system. Here we include several costs:

- The cost of end effector targets  $c_{ee}(q)$ . From the samples generated by  $G$ , we can compute the forward kinematics to obtain the end-effector positions, and compare this to the desired end-effector target (given as the input to the generator).
- The cost of static stability  $c_s(q)$ . To achieve static stability, the center of mass projection on the ground should be located inside the two feet's support polygon.
- The cost of joint limits  $c_l(q)$ . The cost is zero if it is within the limit, and increasing outside the limit.

3) *Output Augmentation*: Instead of feeding the configurations directly to the discriminator, we augment the configurations by some transformations, e.g. end-effector poses. This helps the discriminator to discern between good and bad samples according to the relevant features. Other transformations such as center of mass location can also be added.

4) *Ensemble of networks*: When the desired distributions are multimodal, GAN often converges to only some modes of the distributions. This is known as the Helvetica scenario, or mode collapse [1]. For example, when the desired distributions is a Gaussian Mixture Model, GAN may converge to only some of the mixture components, and not all of them. This is a big problem in robotics context, especially for motion planning, because omitting some portion of the configuration space means reducing the chance of finding valid solutions. To overcome this, we use an ensemble of  $N_{\text{net}}$  neural networks as generator. Given an input, each network generates a corresponding robot configuration, and each one is trained as a stand-alone generator. When the desired distribution is multimodal, different networks may

converge to different modes, enabling us to cover multiple modes. We will show that by doing this, we can cover the distribution better than using a single network.

## B. Inverse Kinematics

For high dimensional robots where analytical IK is not tractable, numerical IK is the standard approach. Given a desired end-effector pose  $x$  and the initial configuration  $q_0$ , an iterative optimization is used to find the value of  $q$  that reaches the pose  $x$ . The Newton–Raphson (NR) root finding method is usually employed to drive the initial guess towards the optimum solution, i.e. to find the root of

$$x - f(q) = 0,$$

where  $f(q)$  is the forward kinematic function for the corresponding end-effector. Starting from the initial guess  $q_0$ , the next solution is obtained by

$$q_{i+1} = q_i - \alpha J^\dagger(x - f(q_i)).$$

In practice, we find it to be quite slow, especially due to the choice of  $\alpha$ . For proper execution, a line search has to be performed to find the good  $\alpha$ , and the regularization for the pseudoinverse  $J^\dagger$  has to be adjusted dynamically.

Instead, we use the quasi-Newton method L-BFGS. We formulate the IK problem as an optimization problem with the corresponding cost functions. For example, in the case of IK for humanoid, we define the cost

$$c(q) = c_{ee}(q) + c_s(q) + c_l(q) + c_p(q),$$

where the subscripts (ee, s, l, p) refer to the end-effector pose, static stability, joint limit, and posture costs. The derivatives can be computed analytically, and we solve this using off-the-shelf L-BFGS algorithm. More details about the cost functions can be found in the appendix.

The computation time for numerical IK really depends on how close the initial guess is to the optimal solution. As discussed in Section III-A, we can obtain good initial guesses by sampling from GAN while giving the end-effector poses as additional inputs to the generator. The resulting configurations would be close to the desired poses and the constraint manifold, reducing the required number of IK iterations significantly.

## C. Constrained Motion Planning

The standard approach in sampling-based constrained motion planning [11] is largely based on RRT, with the addition of the projection step; each sample to be added to the tree is projected first to the constraint manifold. Algorithm III-C describes the steps for constrained RRT (cRRT) for reaching a goal in task space, starting from an initial configuration  $q_0$ . We refer to [11] for more details of the algorithm.

First, we start with a tree  $G$  initialized with the node  $q_0$ . From the given goal task, we compute  $K$  goal configurations (by numerical IK). The following iterations then attempt to extend the tree to one of these goals. At each iteration, a random sample  $q_{\text{rand}}$  is generated and projected to the manifold to obtain  $\hat{q}_{\text{rand}}$ . Nearest neighbor algorithm is used

---

**Algorithm 1** Constrained RRT with goal sampling

---

**INPUT:**  $q_0, x_g$   
**OUTPUT:** the path  $\{q_i\}_{i=0}^T$

```
1:  $G.init(q_0)$ 
2:  $\{q_{g,i}\}_{i=0}^K \leftarrow \text{SampleGoal}(x_g)$ 
3: while  $n < \text{max\_iter}$  do
4:    $q_{\text{rand}} \leftarrow \text{SampleConfig}()$ 
5:    $\hat{q}_{\text{rand}} \leftarrow \text{Project}(q_{\text{rand}})$ 
6:    $q_{\text{near}} \leftarrow \text{NearestNeighbor}(G, \hat{q}_{\text{rand}})$ 
7:    $q_{\text{reached}}^a \leftarrow \text{ConstrainedExtend}(G, q_{\text{near}}, \hat{q}_{\text{rand}})$ 
8:    $q_{g,k} \leftarrow \text{NearestNeighbor}(\{q_{g,i}\}_{i=0}^K, q_{\text{reached}}^a)$ 
9:    $q_{\text{reached}}^b \leftarrow \text{ConstrainedExtend}(G, q_{\text{reached}}^a, q_{g,k})$ 
10:  if  $q_{\text{reached}}^b = q_{g,k}$  then
11:     $P \leftarrow \text{ExtractPath}(T, q_0, q_{g,k})$ 
12:    return  $P$ 
13:  end if
14: end while
```

---

to find the nearest node  $q_{\text{near}}^a$  in the tree, and we then extend the tree from  $q_{\text{near}}^a$  to  $\hat{q}_{\text{rand}}$ . The last configuration obtained from the extension step is denoted as  $q_{\text{reached}}^a$ . Next, we extend the tree from  $q_{\text{reached}}^a$  to one of the goal configurations,  $q_{g,k}$ , chosen to be the one nearest to  $q_{\text{reached}}^a$ . The last configuration obtained from the extension step is denoted as  $q_{\text{reached}}^b$ . If  $q_{\text{reached}}^b$  is equal to  $q_{g,k}$ , we stop the iteration, and compute the path from the root node  $q_0$  to  $q_{g,k}$ . Otherwise, we continue with the next iteration until the goal is reached or the maximum number of iteration is exceeded.

In the extension step, we first linearly interpolate the configurations from  $q_{\text{near}}^a$  to  $\hat{q}_{\text{rand}}$ , project them to the manifold, and check for collision. The extension stops at the first configuration that encounter collision or fail to be projected. We note that in [11], the random sample is not projected to the manifold first, so the interpolation is done towards the random sample  $q_{\text{rand}}$ . We find that it causes the interpolated configurations to be located quite far from the manifold, and hence the number of subsequent projection steps are quite large, while the projected samples are not necessarily continuous or close to one another. Hence, we choose to project the random sample first before doing interpolation. The same way is done in [12].

1) *GAN sampling:* As reported in [12], the projection steps dominate the computation time, more than 95% of the total time. Instead of using uniform sampling, we propose to use the GAN framework to generate the samples. This will give us samples that are already quite close to the manifold, hence reducing the computation time significantly.

To generate samples from the GAN framework, we first determine the task space region of interest, i.e. a box that covers the reachable points of the robot's end-effector. We sample points inside this box, and use it as the target for the generator. Together with the Gaussian noise, we can then obtain a set of configurations that are near to the target, and require fewer projection steps. As the generator consists of  $N_{\text{net}}$  neural networks, we choose one out of the  $N_{\text{net}}$  configurations randomly as the output of the sampler.

## IV. EXPERIMENTAL RESULTS

We implemented the proposed method<sup>1</sup> on two systems: the 7-DoF Panda and 28-DoF Talos. The dataset is created by randomly sampling configurations and then projecting it to the constraints manifold. The generator consists of  $N_{\text{net}} = 10$  neural networks with 2 hidden layers, each has 200 nodes, while the discriminator is a neural network with 2 hidden layers (each has 20 nodes for Panda and 40 nodes for Talos). ReLu is used as the activation function. We train the networks using SGD.

### A. Projection and Inverse Kinematics (IK)

As described in Section III-B, the IK is formulated as an optimization problem by defining several cost functions that consist of the terms associated to the constraints (e.g. joint limit, end-effector orientation) and the task, e.g. end-effector (EE) position. The optimization problem is solved using L-BFGS algorithm. We compare initializing the IK by GAN versus random sampling. For each cost function, we set a certain threshold, and the optimization is run until all costs are below the thresholds.

a) *Panda:* Panda's configuration consists of 7 joint angles. For IK, the cost functions consists of 3 terms: a) joint limit, b) EE orientation constraint, and c) EE position. The orientation is constrained to face upward. For the projection, there is no cost on the EE position, but we add a posture cost that regularizes around a nominal configuration.

b) *Talos:* Talos' configuration consists of 28 joint angles (7 for each arm, 6 for each leg, and 2 for the torso) and 3 base position (we keep the base orientation fixed). For IK, the cost function consists of the following terms: a) joint limit, b) static stability (the COM projection on the ground must be within the support polygon defined by the two feet), c) the posture cost, d) the feet pose, and d) the right hand position. The nominal posture is the initial configuration given to the IK solver, except for the left hand, which is regularized around a default posture. The EE is set to be the right hand. The feet are constrained to remain at the same location. The task is to reach the desired location of the right hand, while respecting the constraints. For the projection, we omit the cost on the EE position.

We sample  $N = 500$  tasks. The average result is shown in Table I.  $T_{\text{ave}}$  is the average computation time when considering all tasks, while  $T_{\text{ave}}^*$  and  $P^*$  denote the average computation time and the number of projection steps when only considering the tasks that are successful. We can see that using GAN speeds up both projection and IK computation significantly, around 2-3 times faster than random sampling, even when considering only the successful results. Random sampling has lower success rate, as can be expected for a nonlinear optimization problem (starting far from the optimal solution reduces the success rate). When the optimization cannot find the solution, it continues optimizing until convergence or reaching the maximum iteration, spending high

<sup>1</sup>The codes are provided in [https://github.com/teguSL/learning\\_distribution\\_gan](https://github.com/teguSL/learning_distribution_gan).

TABLE I

COMPARING PROJECTION AND IK INITIALIZED BY RANDOM SAMPLING VS GAN SAMPLING. THE ASTERISK SIGNIFIES THAT THE CORRESPONDING VALUES ARE COMPUTED ONLY FOR THE SUCCESSFUL TRIALS.

Robot	Task	Method	Success	$T_{ave}(ms)$	$T_{ave}^*(ms)$	$P^*$
Panda	Projection	Random	84.6	$6.8 \pm 6.4$	$4.6 \pm 3.0$	$14.1 \pm 9.9$
		GAN	<b>98.4</b>	<b>2.3 <math>\pm</math> 2.6</b>	<b>2.1 <math>\pm</math> 2.0</b>	<b>5.7 <math>\pm</math> 6.3</b>
	IK	Random	64.8	$11.9 \pm 8.6$	$7.5 \pm 5.1$	$27.8 \pm 19.9$
		GAN	<b>89.2</b>	<b>6.4 <math>\pm</math> 6.6</b>	<b>4.5 <math>\pm</math> 3.2</b>	<b>16.1 <math>\pm</math> 12.5</b>
Talos	Projection	Random	85.8	$25.5 \pm 40.1$	$9.3 \pm 2.3$	$27.5 \pm 6.8$
		GAN	<b>100.0</b>	<b>2.9 <math>\pm</math> 1.6</b>	<b>2.9 <math>\pm</math> 1.6</b>	<b>8.7 <math>\pm</math> 4.8</b>
	IK	Random	83.6	$82.7 \pm 85.8$	$46.1 \pm 24.7$	$56.0 \pm 29.7$
		GAN	<b>100.0</b>	<b>12.3 <math>\pm</math> 8.4</b>	<b>12.3 <math>\pm</math> 8.4</b>	<b>14.3 <math>\pm</math> 9.5</b>

TABLE II

COMPARING CONSTRAINED RRT USING RANDOM SAMPLING VS GAN SAMPLING

Robot	Method	Success	$T_{ave}(s)$	$P$	$E$
Talos (Task 1)	Random	100.0	$2.87 \pm 2.22$	$1781.3 \pm 1408.5$	$17.4 \pm 14.4$
	GAN	100.0	<b>0.66 <math>\pm</math> 0.31</b>	<b>567.1 <math>\pm</math> 275.5</b>	<b>15.1 <math>\pm</math> 9.6</b>
Talos (Task 2)	Random	100.0	$7.50 \pm 9.53$	$4303.6 \pm 5433.0$	<b>51.2 <math>\pm</math> 63.6</b>
	GAN	100.0	<b>1.90 <math>\pm</math> 1.38</b>	<b>1522.6 <math>\pm</math> 1129.6</b>	$57.1 \pm 50.1$
Talos (Task 3)	Random	97.0	$26.31 \pm 26.38$	$12595.8 \pm 12319.8$	$226.9 \pm 259.6$
	GAN	96.0	<b>2.59 <math>\pm</math> 3.42</b>	<b>1709.7 <math>\pm</math> 2489.4</b>	<b>75.8 <math>\pm</math> 170.0</b>

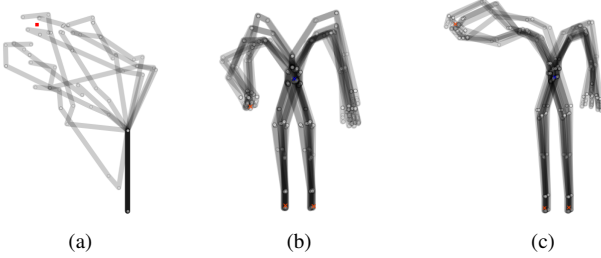


Fig. 3. Samples generated by GAN for Panda (a) and Talos (b) and (c)). The samples correspond to the desired end-effector positions, shown in red in the figure. We can see that GAN manages to generate multimodal configurations.

computational time (namely,  $T_{ave}$  is higher than  $T_{ave}^*$ ). In practice,  $T_{ave}$  is the one we actually observe, since there is no way to avoid bad random samples.

The more complex the problem is, the more advantageous the GAN framework is. Comparing the result between Panda and Talos, we see that the benefit of GAN is higher in the case of Talos, i.e. the average computational time is around 3 times higher than random sampling. This is because in such a high DoF system, random sampling would struggle to get good performance, and when it fails to find a solution it will spend high computational time, as can be seen with  $T_{ave}$ .

We claim that using an ensemble of networks increases the coverage of the distribution, especially when it is multimodal. Fig. 3 shows samples generated by GAN, by giving some desired EE position (shown in red). We can see that in both robots, the generated samples belong to multiple modes. This is relevant for both IK (as it can help us find multiple solutions more easily), and in motion planning (as better

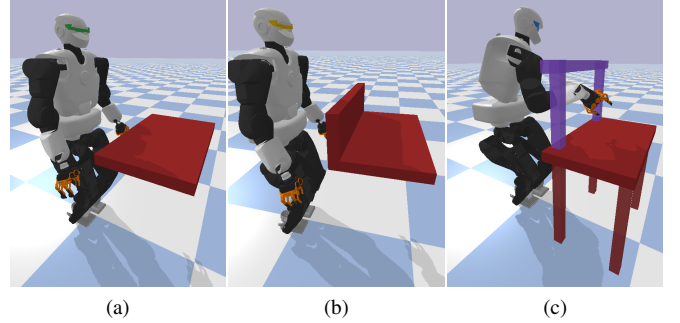


Fig. 4. Three constrained motion planning tasks (with increasing complexity) for Talos are given in (a), (b) and (c). The initial configuration starts with the right arm above the table, and the task is to reach a location below the table while avoiding obstacles.

coverage of the distribution means higher success rate).

Besides the quantitative results shown in Table I and II, we observe that GAN produces configurations that are still close to the manifold even when the target is infeasible, i.e. too far from the arm reach (Fig. 1b). Additionally, we can also extend the target variables to include the left hand, so that we can do approximate IK for all the four limbs simultaneously using GAN (Fig. 1c). We refer to the supplementary video for a better visualization of the infeasible target IK, the multi-limbs IK, and the multimodal solution.

### B. Motion Planning

We use the GAN sampling for sampling-based constrained motion planning, as described in Algorithm 1. We consider three different environments in Fig. 4a-c, in increasingly more difficult order, similar to the ones used in [12]. The task is to move from a random initial configuration above a table to reach a specified target position with the right

hand below the table, while satisfying the static stability and joint limits. For each environment, we run  $N = 100$  random tasks for comparison. We compute  $K = 10$  goal configuration for each task. The result can be seen in Table II.  $T_{\text{ave}}$ ,  $P$ , and  $E$  denote the average planning time, the number of projection steps, and the number of extension steps in planning (*ConstrainedExtend* in Algorithm 1). Even in the easiest task, i.e. Task 1, planning with GAN sampling is more than 4 times faster than random sampling. The number of extension steps is actually similar, so the gain in computation time is really due to the fewer projection steps necessary for samples generated by GAN (see the column of  $P$ : for a similar number of extension steps, the required projection for GAN samples is 4 times smaller than random samples).

While in Task 1 and Task 2 the number of extension steps  $E$  is similar, in Task 3 (the most difficult one due to the tight obstacles) random sampling has much higher costs. We observe that random sampling often struggles to produce certain configurations, e.g. where the right hand is below the table. Although random sampling is supposed to cover the configuration space uniformly, with the projection step it becomes more complicated, and some region of the task space is less often reached than others. GAN samples do not have this issue, as the samples are generated by first sampling random locations in task space and then computing the configurations associated to these locations. The result is that in Task 3, GAN outperforms the random sampling (more than 10 times faster). The good performance is also due to the usage of ensemble networks instead of a single network for the generator. If only one network is used, the planning cannot succeed in most cases because the samples are limited to some particular modes.

### C. Discussion

From the results, we see that GAN enables us to generate good quality samples close to the desired manifold, even when using a quite basic GAN structure. Since it is a very flexible tool, there are a lot of potential improvements that can be pursued in future work. As done in [7], if we generate many planning data in a given environment, we can condition GAN on initial and goal configurations to obtain samples that are relevant for the task, instead of trying to cover the whole distributions. GAN also works well with high dimensional inputs such as images, so that it would be possible to train the GAN with some environment representation (e.g. voxel data or depth image) to generate samples that avoid collisions in different environments. Since GAN can be conditioned on the desired target location, it is possible to use it for generating biased samples in task space.

In this paper, we use an ensemble of networks as generator to cover the multimodal distribution. While this works very well in our application, there is no guarantee that it will cover all the modes in the actual distribution. For the sampling-based motion planning, a simple strategy to overcome this is to also do uniform sampling with some specified probability (e.g. 20% of the time) in addition to GAN sampling. This will keep the probabilistic completeness property of the al-

gorithm. There are also other methods that attempt to handle this mode collapse issue, e.g. using minibatch features [17] or unrolled GANs [18].

## V. CONCLUSION

We have presented a framework using GAN to learn the distribution of valid robot configurations under various constraints. The method is then used for inverse kinematics and sampling-based constrained motion planning to speed up computational time. We validate the proposed method on two simulated platforms: 7-DoF manipulator Panda, and 28-DoF humanoid robot Talos. We show that in all settings, the proposed method manages to reduce the computational time significantly (up to 10 times faster). The method is very general and easily applicable to other robotic systems.

## APPENDIX

### A. Cost Functions for IK

The IK problem is formulated as an unconstrained optimization problem. Both the constraints (e.g. static stability, joint limit) and the tasks (the end-effector position) are implemented as cost functions, weighted according to their importance. We list here several cost functions that we use. Note that the derivative of these costs can be computed analytically. We use the fast rigid body dynamic library *pinocchio* [19] to compute the forward kinematics and the cost derivatives.

#### 1) End-effector pose cost:

$$c_{\text{ee}}(\mathbf{q}) = (\mathbf{p}(\mathbf{q}) - \mathbf{p}_{\text{ref}})^{\top} \mathbf{W} (\mathbf{p}(\mathbf{q}) - \mathbf{p}_{\text{ref}}). \quad (1)$$

$c_{\text{ee}}(\mathbf{q})$  penalizes the deviation of the end-effector pose from the given reference pose. We use this both for the constraints (Talos' feet location) and the task (Talos' right hand and Panda's gripper). We use the quadratic penalty on the error, where  $\mathbf{p}(\mathbf{q})$ ,  $\mathbf{p}_{\text{ref}}$  are the end-effector pose and the reference pose, respectively.  $\mathbf{W}$  is the diagonal weight matrix.

#### 2) Posture cost:

$$c_p(\mathbf{q}) = (\mathbf{q} - \mathbf{q}_{\text{nom}})^{\top} \mathbf{W} (\mathbf{q} - \mathbf{q}_{\text{nom}}). \quad (2)$$

$c_p(\mathbf{q})$  penalizes the configuration  $\mathbf{q}$  from a nominal configuration  $\mathbf{q}_{\text{nom}}$ . In this paper we often use the initial values given to the projector as  $\mathbf{q}_{\text{nom}}$ , so that the projector will project the configuration to the manifold while keeping it as close as possible to the initial configuration. This is especially important for the *ConstrainedExtend* step, because without this, the interpolated configurations may be projected differently, causing them to be discontinuous.

3) *Quadratic barrier function*: For the subsequent costs, i.e. joint limit and static stability, we first define a quadratic barrier function  $f_b(\mathbf{x})$ . Given a variable  $\mathbf{x}$ , the lower limit  $\mathbf{l}_b$  and upper limit  $\mathbf{l}_u$ , the function is defined as

$$\begin{aligned} \mathbf{r}_b(\mathbf{x}) &= \min(\mathbf{x} - \mathbf{l}_b, \mathbf{0}), \\ \mathbf{r}_u(\mathbf{x}) &= \max(\mathbf{x} - \mathbf{l}_u, \mathbf{0}), \\ f_b(\mathbf{x}, \mathbf{l}_b, \mathbf{l}_u) &= 0.5(\mathbf{r}_b(\mathbf{x})^2 + \mathbf{r}_u(\mathbf{x})^2), \end{aligned}$$

where  $\mathbf{r}_b$  and  $\mathbf{r}_u$  are the violations with respect to the lower and upper limits, and  $\mathbf{0}$  is a zero vector.



4) *Joint limit cost*: Given the joint lower and upper limit ( $l_b, l_u$ ), the cost associated to the joint limit is given as

$$c_l(\mathbf{q}) = f_b(\mathbf{q}, l_b, l_u). \quad (3)$$

5) *Static stability cost*: To achieve static stability, the center of mass (CoM) projection on the ground should fall on the support polygon formed by the feet. We approximate this polygon by a rectangle surrounding the feet. The lower and upper limit of the horizontal CoM values, ( $l_b, l_u$ ), are given by this rectangle. The cost is given as

$$c_s(\mathbf{q}) = f_b(\mathbf{p}_{\text{com}}(\mathbf{q}), l_b, l_u), \quad (4)$$

where  $\mathbf{p}_{\text{com}}$  is the center of mass at the configuration  $\mathbf{q}$ .

6) *Optimization stopping criteria*: Conceptually, starting from a good initial guess would speed up the optimization significantly, as compared to starting from a random initial guess. However, this is not necessarily true in practice, as it depends on the optimization setup. Standard optimization tool such as *scipy* uses the convergence of either the cost function values or its gradient as the stopping criteria. The optimization is terminated when the change in these values is below the specified threshold. Under this condition, we found that even starting from a good initial guess still ends up with a lot of optimization steps, as the solver still tries to refine the solution until convergence.

In contrary, we specify a desired threshold for each cost function, and at each optimization step, we check if the cost values (not the change between the current and previous values) are below these thresholds. If they are, we stop the optimization. This better suits our requirement because when these threshold are satisfied, the solution is already acceptable and we do not need to run the optimizer until convergence. With this setup, the advantage of initializing from a good guess becomes greater (up to 3–4 times gain in speed), while still being practically good.

### B. GAN on 2-DoF robot example

The advantage of using an ensemble of networks as the generator can clearly be seen using a 2-link robot example. Fig. 5a shows the setup of the robot surrounded by obstacles. The configuration consists of the two joint angles. The valid configurations (i.e. the ones without collision) are plotted in Fig. 5b and Fig. 5c as red circles, and we try to learn this distribution using GAN. When using only one network for the generator, GAN converges to only some part of the configuration space, as depicted in Fig. 5b (the GAN samples are plotted as blue crosses). Using  $N_{\text{net}} = 5$  networks, we manage to cover most of the configuration space (Fig. 5c).

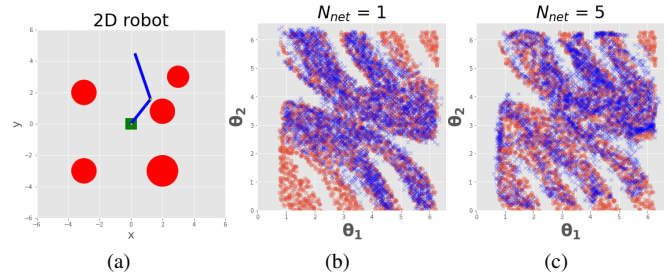


Fig. 5. Illustrative example of a 2-DoF robot with obstacles. (a) shows the robot with circular obstacles. The configurations (i.e. joint angles) that are not in collision are plotted in (b) and (c) as red circles. We try to learn this distribution using GAN. In (b), we use one neural network as the generator, and the GAN samples are plotted as blue crosses. We see that the samples do not cover the whole distribution. Using an ensemble of 5 networks in (c), we manage to cover most of the distribution.

### REFERENCES

- [1] I. Goodfellow, “Nips 2016 tutorial: Generative adversarial networks,” *arXiv preprint arXiv:1701.00160*, 2016.
- [2] C. Ledig, L. Theis, F. Huszar, J. Caballero, A. Cunningham, A. Acosta, A. Aitken, A. Tejani, J. Totz, Z. Wang, *et al.*, “Photo-realistic single image super-resolution using a generative adversarial network,” in *Proc. IEEE Intl Conf. on Computer Vision and Pattern Recognition (CVPR)*, 2017, pp. 4681–4690.
- [3] S. Reed, Z. Akata, X. Yan, L. Logeswaran, B. Schiele, and H. Lee, “Generative adversarial text to image synthesis,” in *Proc. Intl Conf. on Machine Learning*, vol. 48, 2016, pp. 1060–1069.
- [4] J.-Y. Zhu, P. Krähenbühl, E. Shechtman, and A. A. Efros, “Generative visual manipulation on the natural image manifold,” in *European conference on computer vision*. Springer, 2016, pp. 597–613.
- [5] P. Lehner and A. Albu-Schäffer, “Repetition sampling for efficiently planning similar constrained manipulation tasks,” in *Proc. IEEE/RSJ Intl Conf. on Intelligent Robots and Systems (IROS)*, 2017, pp. 2851–2856.
- [6] —, “The repetition roadmap for repetitive constrained motion planning,” *IEEE Robotics and Automation Letters (RA-L)*, vol. 3, no. 4, pp. 3884–3891, 2018.
- [7] B. Ichter, J. Harrison, and M. Pavone, “Learning sampling distributions for robot motion planning,” in *Proc. IEEE Intl Conf. on Robotics and Automation (ICRA)*, 2018, pp. 7087–7094.
- [8] D. Holden, J. Saito, T. Komura, and T. Joyce, “Learning motion manifolds with convolutional autoencoders,” in *SIGGRAPH Asia 2015 Technical Briefs*, 2015, pp. 1–4.
- [9] Z. Kingston, M. Moll, and L. E. Kavraki, “Sampling-based methods for motion planning with constraints,” *Annual review of control, robotics, and autonomous systems*, vol. 1, pp. 159–185, 2018.
- [10] D. Berenson, S. S. Srinivasa, D. Ferguson, and J. J. Kuffner, “Manipulation planning on constraint manifolds,” in *Proc. IEEE Intl Conf. on Robotics and Automation (ICRA)*, 2009, pp. 625–632.
- [11] D. Berenson, S. Srinivasa, and J. Kuffner, “Task space regions: A framework for pose-constrained manipulation planning,” *Intl Journal of Robotics Research*, vol. 30, no. 12, pp. 1435–1460, 2011.
- [12] Y. Yang, V. Ivan, W. Merkt, and S. Vijayakumar, “Scaling sampling-based motion planning to humanoid robots,” in *2016 IEEE International Conference on Robotics and Biomimetics (ROBIO)*, 2016, pp. 1448–1454.
- [13] M. Stilman, “Global manipulation planning in robot joint space with task constraints,” *IEEE Transactions on Robotics*, vol. 26, no. 3, pp. 576–584, 2010.
- [14] F. Kanehiro, E. Yoshida, and K. Yokoi, “Efficient reaching motion planning and execution for exploration by humanoid robots,” in *Proc. IEEE/RSJ Intl Conf. on Intelligent Robots and Systems (IROS)*, 2012, pp. 1911–1916.
- [15] J. Schulman, J. Ho, A. Lee, I. Awwal, H. Bradlow, and P. Abbeel, “Finding locally optimal, collision-free trajectories with sequential convex optimization,” in *Proc. Robotics: Science and Systems (R:SS)*, 2013.
- [16] T. S. Lembono, A. Paolillo, E. Pignat, and S. Calinon, “Memory of motion for warm-starting trajectory optimization,” *IEEE Robotics and Automation Letters (RA-L)*, vol. 5, no. 2, pp. 2594–2601, 2020.
- [17] T. Salimans, I. Goodfellow, W. Zaremba, V. Cheung, A. Radford, and X. Chen, “Improved techniques for training gans,” in *Advances in Neural Information Processing Systems (NIPS)*, 2016, pp. 2234–2242.
- [18] M.-Y. Liu and O. Tuzel, “Coupled generative adversarial networks,” in *Advances in Neural Information Processing Systems (NIPS)*, 2016, pp. 469–477.
- [19] J. Carpentier, F. Valenza, N. Mansard, *et al.*, “Pinocchio: fast forward and inverse dynamics for poly-articulated systems,” <https://stack-of-tasks.github.io/pinocchio>, 2015–2019.